Density Limit Studies in the Large Helical Device

B. J. Peterson 1), J. Miyazawa 1), K. Nishimura 1), S. Masuzaki 1), Y. Nagayama 1), N. Ohyabu 1), H. Yamada 1), K. Yamazaki 1), T. Kato 1), N. Ashikawa 1), R. Sakamoto 1), M. Goto 1), K. Narihara 1), M. Osakabe 1), K. Tanaka 1), T. Tokuzawa 1), M. Shoji 1), H. Funaba 1), S. Morita 1), T. Morisaki 1), O. Kaneko 1), K. Kawahata 1), A. Komori 1), S. Sudo 1), O. Motojima 1) and the LHD Experimental Group 1)

1) National Institute for Fusion Science, Toki-shi, Gifu-ken 509-5292 JAPAN

e-mail contact of main author: peterson@LHD.nifs.ac.jp

Abstract.

Steady state densities of up to $1.6 \times 10^{20} m^{-3}$ have been sustained using gas puff fuelling and NBI heating up to 11 MW in the Large Helical Device (LHD). The density limit in LHD is observed to be ~ 1.4 times the Sudo limit. The density is ultimately limited by radiative collapse which is attributed to the onset of a radiative thermal instability of the light impurities in the edge region of the plasma based on several observations. First of all the onset of the radiative thermal instability is tied to a certain edge temperature threshold. Secondly, the onset of thermal instability occurs first in oxygen and then carbon as expected from their cooling rate temperature dependencies. Finally, radiation profiles show that as the temperature drops and the plasma collapses the radiating zone broadens and moves inward. In addition, comparison with the total radiated power behaviour indicates that Carbon is the dominant radiator. Comparison of modelling with images of radiation brightness from imaging bolometers indicates that the poloidal asymmetry which accompanies the radiative collapse is toroidally symmetric. Other than the operational density limit where the discharge is terminated by radiative collapse, a confinement limit has been recognized in LHD. This confinement limit appears at lower density than the operational density limit, similar to the saturated ohmic confinement observed in tokamaks. To investigate the physics behind this degradation, the parameter dependence of the thermal diffusivity, c, has been investigated. While the temperature dependence in ISS95 is as strong as the gyro-Bohm model of $c \propto T_e^{1.5}$, weaker T_e dependence of $c \propto T_e^{0.5}$ appears in the high-density regime. Such weak T_e dependence results in the weak density dependence of the global energy confinement as $t_E \propto \bar{n}_e^{1/3}$.

1. Introduction

Density limit is an important issue for future fusion reactors since the fusion reaction rate is a function of the density squared. In tokamaks an empirical density limit (Greenwald limit) has been observed which scales with the plasma current density. Densities above the Greenwald limit have been achieved primarily in tokamaks using pellet injection to achieve peaked density profiles, indicating that the density limiting process is related to the physics of the edge plasmas. As the density limit in a tokamak is approached the MARFE phenomenon is commonly observed and the discharge is ultimately terminated by a current disruption which can cause considerable damage to the device from induced currents and runaway electrons [1].

On the other hand, the operational density in stellarators is not limited by current disruption as in tokamaks, nor is the Greenwald limit directly applicable to net-current free plasmas. Studies on Heliotron-E resulted in an empirical density limit scaling law (Sudo limit) which is proportional to the square root of the product of the input power density and the magnetic field [2]. In the W7-AS stellarator, using a graphite limiter configuration, the density limit was attributed to power imbalance due to strong radiation from heavy impurities from the core of the plasma. This study also revealed a density limit scaling law very similar to the Sudo limit [3]. With the addition of a graphite island divertor in W7-AS, at high densities the radiation profile became hollow with the pumping out of impurities from the core and much higher steady state densities of up to 3.5 x 10^{20} m^{-3} could be achieved. However, when the higher deposited power was considered the previously derived scaling law was still obeyed [4].

Initial investigations into the density limit on LHD [5] have shown that the density in LHD is limited by a radiative thermal instability which results in the collapse of the plasma at a limit which is 1.4 times the Sudo limit. This collapse is characterized by a poloidal asymmetry in the radiation and density with the high density and high radiation region on the inboard side. Further investigation of this phenomenon showed that the poloidal asymmetry also appears in the electron temperature profiles (lower temperature on the inboard side) as the plasma column contracts [6]. Measurements with imaging bolometers indicated that the radiation asymmetry was located on the inboard side slightly below the midplane [7]. Also, after boronization of the vacuum vessel wall, indeed, the radiation loss, P_{rad}, decreases about 20 ~ 50 %, compared at similar density and input power, P_{abs}, and the density limit increases 20 ~ 50 % [8]. These results indicate the importance of P_{rad} on density limit studies. However, the thermal instability is typically triggered even when P_{rad} is less than a half of P_{abs}. These observations call for an investigation of the role of P_{rad} and the exploration of the mechanism which triggers or enhances the thermal instability.

Confinement properties in the high-density region are also important as degradation of confinement in the edge region may be related to the onset of the thermal instability. Other than the operational density limit where the discharge is terminated by radiative collapse, a confinement limit has been recognized in LHD. The energy confinement times, t_{E}, of the moderate density LHD plasmas are well reproduced by the international stellarator scaling 95 (ISS95), which has strong positive density dependence as $t_{\mathrm{E}} \propto \bar{n}_{\mathrm{e}}^{0.51}$. In the high-density regime, however, the energy confinement is lower than the prediction of ISS95. This confinement limit appears at lower density than the operational density limit, similar to the saturated ohmic confinement observed in tokamaks. To investigate the physics behind this degradation, the parameter dependence of the thermal diffusivity, c, is investigated.

In this paper we expand on this research reporting the most recent results of efforts to increase the density in LHD and investigating the density limit from various perspectives including the plasma behaviour in the divertor region, confinement degradation at high density, etc.

2. Peak density parameters and scaling in LHD

In the latest experimental campaign in the Large Helical Device (LHD), line-averaged densities of up to $1.6 \times 10^{20} \mathrm{m}^{-3}$ have been sustained for more than 0.7 s by 11 MW neutral beam injection using gas puff fuelling. An example of one of these high density discharges is shown in Figure 1. This value of density corresponds to 1.36 times Sudo scaling, which is close to what was observed peviously. In addition, using multiple hydrogen pellets, the density has been increased to over $2 \times 10^{20} \mathrm{m}^{-3}$ transiently as shown in Figure 2.
Data from the most recent campaign also shows a limit which exceeds the Sudo limit by a factor of approximately 1.4 (see Figure 3) as was seen in previous studies [5,6].

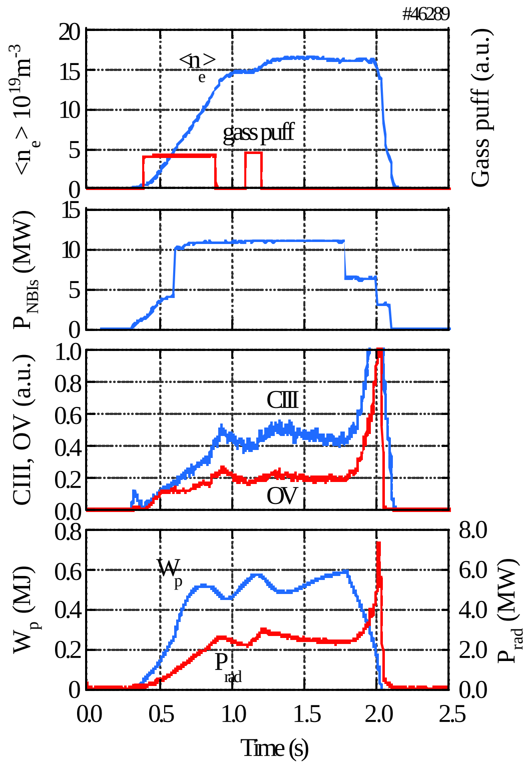

Fig. 1. Typical waveforms of a high density discharge using gas puff fuelling (shot #46289) (a) line-averaged density and gas-puff timing, (b) deposited NBI power, (c) spectroscopy signals from OV and CIII, and (d) total plasma stored energy and total radiated power.

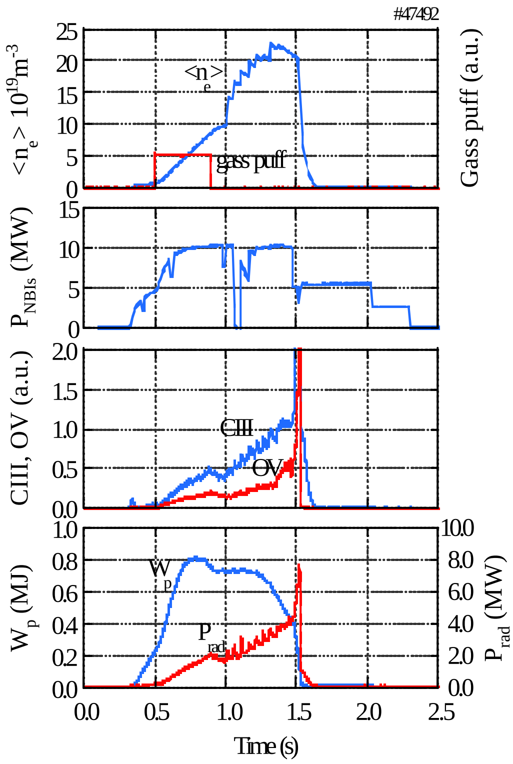

Fig. 2. Typical waveforms of a high density discharge using gas puff and hydrogen pellet fuelling (shot #47492) (a) line-averaged density and gas-puff timing, (b) deposited NBI power, (c) spectroscopy signals from OV and CIII, and (d) total plasma stored energy and total radiated power.

3. Evolution of parameters leading to radiative collapse at the density limit

3.1 Evolution of bulk parameters

The terminal phase of a typical discharge with radiative collapse is shown in Fig. 4. During the steady state portion of the discharge prior to 2 s, the radiation is proportional to the line-averaged density, $\bar{n}_e$. This phase ends when the radiative thermal instability is triggered as indicated by the sharp increases in P_{rad} and the light impurities emission. After this point the radiation increases rapidly and its dependence on the density becomes stronger than linear (as seen in Figure 5) as the plasma column starts to contract. The critical time (t_c = 2.1 s in Fig. 4 and Fig. 5) of the onset of the thermal instability is defined when P_{rad} is proportional to $\bar{n}_e^{\,3}$ (see Fig. 4(e) and Fig. 5,

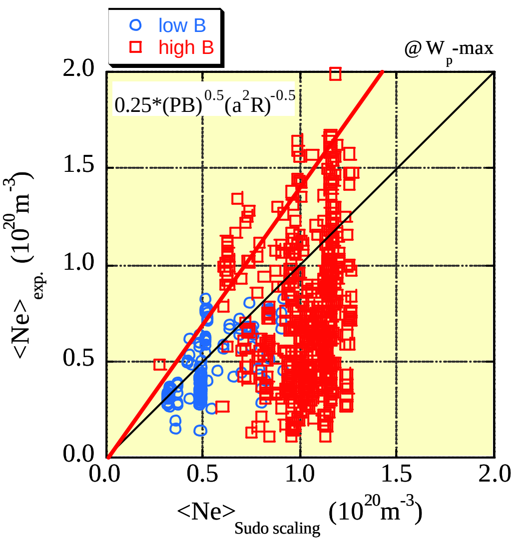

Fig. 3. Density limit scaling for LHD data taken at the timing of maximum stored energy plotted versus the Sudo limit. Red line indicates a factor of 1.4

where $x = (dP_{rad}/dt/P_{rad}) / (d\bar{n}_e/dt/\bar{n}_e)$, which we call the density exponent given by $P_{rad} = \bar{n}_e^{\,x}$). At this time the edge (at $r = r/a = 0.9$) temperature is consistently observed to decrease to about 150 eV regardless of the input power and plasma density as is seen in Fig. 6. This characteristic edge temperature is insensitive to P_{abs} and $\bar{n}_e$ as long as the wall condition is maintained, confirming that the onset of the thermal instability is closely tied to the edge plasma temperature. After t_c the temperature at $r = 1$ has dropped below the measurable limit of 50 eV, which is the temperature below which the oxygen radiation grows rapidly leading to the onset of the radiative thermal instability as seen in Fig. 4(c) followed ~ 50 ms later by C_{III} which becomes unstable at a lower electron

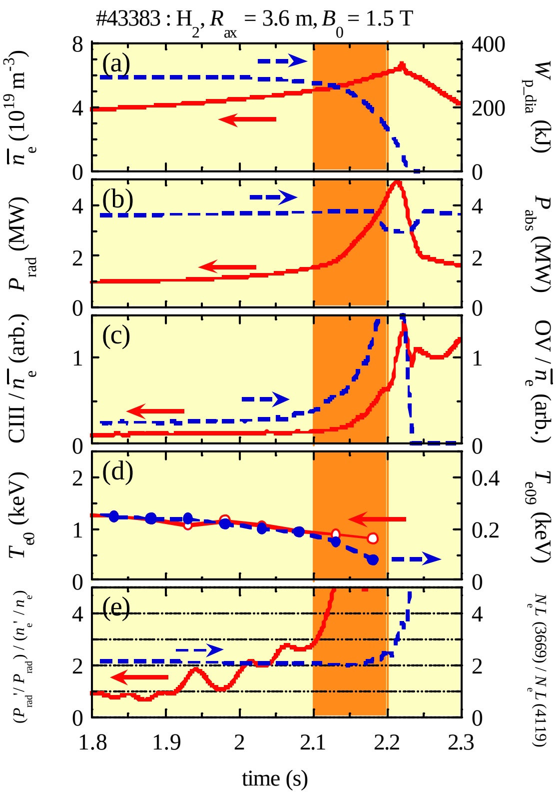

Fig. 4 Typical waveforms of a discharge terminated by radiative collapse in LHD.

temperature. The radiation is also enhanced after t_c as the hot plasma column shrinks leaving an increasingly larger volume of low temperature plasma in which the light impurities radiate

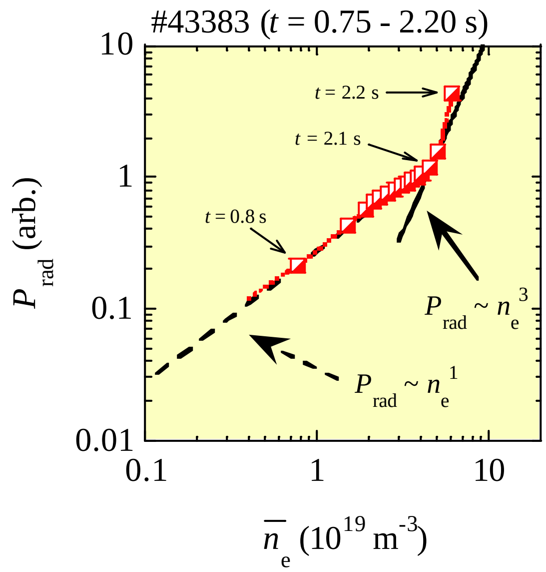

Fig. 5 Radiated power dependence on density

strongly. After t_c the edge temperature decreases faster than that at the core (Fig. 4(d)), presumably due to radiative cooling in the edge by light impurities. Comparison of the growth rate of the O_V radiation in Fig. 4(c) with the decay rate of the stored energy in Fig. 4(a) also indicates that the edge radiative losses are responsible for the confinement degradation.

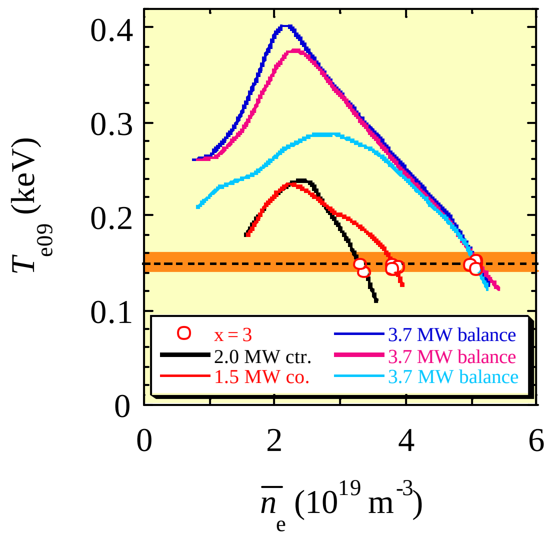

Fig. 6 Edge electron temperature dependence on density for varying input powers.

3.2 Edge parameters and role of impurities

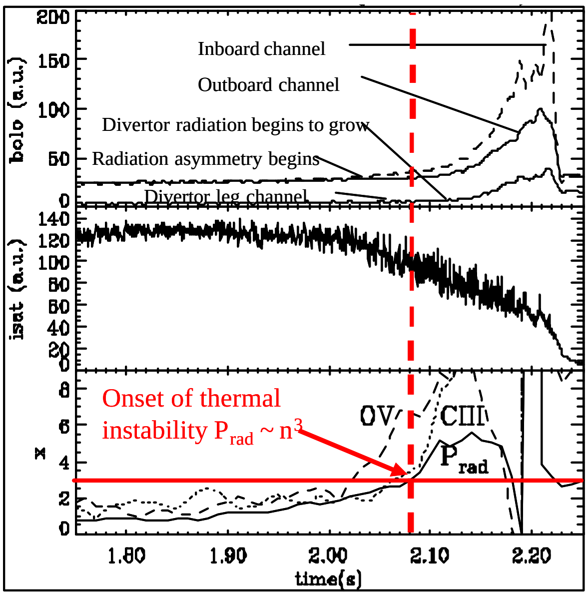

Fig. 7 Time evolution of bolometer brightness, divertor ion saturation current, and the densty exponent for the total radiated power, CIII and OV data shown in Fig. 4.

Since the dominant intrinsic light impurities are oxygen and carbon they should be responsible for the strong increase in the radiation from the edge. First we consider the radiation brightness from the divertor, core and edge plasmas in Fig. 7 as the discharge shown in Fig. 4 collapses. One notes that the onset of the thermal instability, as defined by the red dashed line when x = 3 for the total radiation, is followed by the development of the previously observed asymmetry in the radiation as the radiation from the inboard channel starts to diverge from the channel located near the outboard edge of the plasma. At the same time the radiation from the divertor leg region is increasing, but not as dramatically as the radiation form the inboard side. The ion-saturation current from the divertor probe begins to drop with the onset of the thermal instability and the radiation asymmetry as it approaches a detached state. Finally, considering the density exponents of the light impurities signals, CIII and OV, and the radiated power, one notes that the thermal instability begins in the OV, but that the CIII signal most closely matches the total radiated power indicating that the carbon is the dominant impurity. This temporal progression makes sense in that the oxygen should radiate at a higher temperature, and therefore the thermal instability should begin earlier in the oxygen as the edge temperature drops. Also, the above suggestion, that carbon is the dominant impurity, is consistent with observations before and after boronization, that while the reduction of OV radiation is stronger than that seen in the reduction of CIII, the reduction in CIII more closely matches the reduction in the total radiated power [8].

3.3 Evolution of radiation profiles during collapse

In Fig. 8 the evolution of the radiated power density profile from the bolometer array at the horizontally elongated cross-section [9] is shown. In the steady state portion of the discharge the profile is hollow. After the onset of the thermal instability the strongly radiating zone broadens and moves inward minor radially. Also one notes some indication of growth in the core radiation. At the edge of the plasma one notes the radiation reaches a maximum then decreases, then increases again. This is also seen in the inboard channel of the bolometer in Fig. 8 and may be related to the two peaks observed in the cooling rate of the impurities as a function of electron temperature. One should take care in the quantitative evaluation of the radiation profile during the collapsing phase as the asymmetry in the radiation signal may lead to errors in the tomographic inversion. These errors should be mitigated in this case by the orientation of the array which fans out vertically while the asymmetry has an inboard-outboard nature.

3.4 Radiation asymmetry at collapse

As was seen in Fig. 8 and as was reported previously [5,6,7] a MARFE-like asymmetry is observed during the radiative collapse in various diagnostics including two resistive bolometer arrays, Thomson scattering and the FIR interferometer, each located at a different toroidal angle spread through one half of the torus. All of these diagnostics indicate that the low temperature, high density, high radiation region is located on the inboard side, suggesting that this poloidally asymmetric feature is toroidally symmetric. In Fig. 9 we show the results of two imaging bolometers [9] at two different times, compared with images calculated from models of the radiation. The left hand set of images come from the steady state period of the discharge which has a poloidally and toroidally symmetric hollow profile which is confirmed by the images calculated from a toroidally and poloidally symmetric hollow radiation profile. In the left hand set of images, the data from the imaging bolometers taken from later in the same discharge during the radiative collapse are compared with images calculated from the same hollow profile multiplied by a poloidally asymmetric (yet toroidally symmetric) term given as

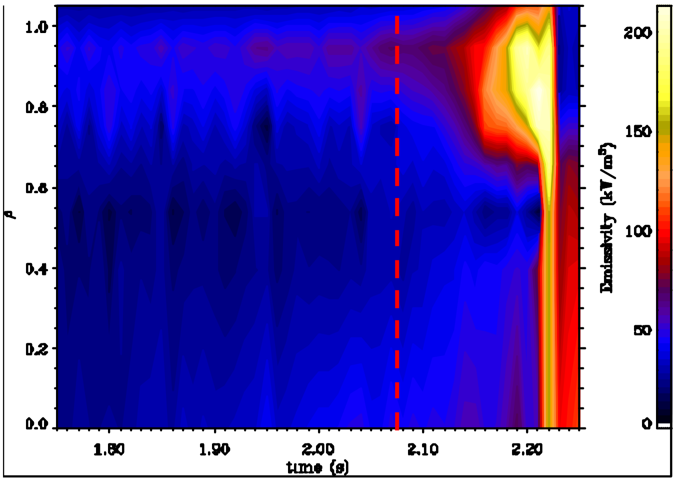

Fig. 8 Evolution of radiated power density profile during radiative collapse of shot43383. Red dashed line indicates the onset of the radiative instability (x = 3).

$$S(r,q) = S(r)\cdot[1+F(q)] \quad \text{and} \quad F(q) = \left((1+\cos(q+150))/2\right)^{50}.$$

The comparison of this model with the data taken together with the results for the other diagnostics mentioned above indicates that that this phenomenon is toroidally symmetric, which is another aspect which it has in common with a MARFE.

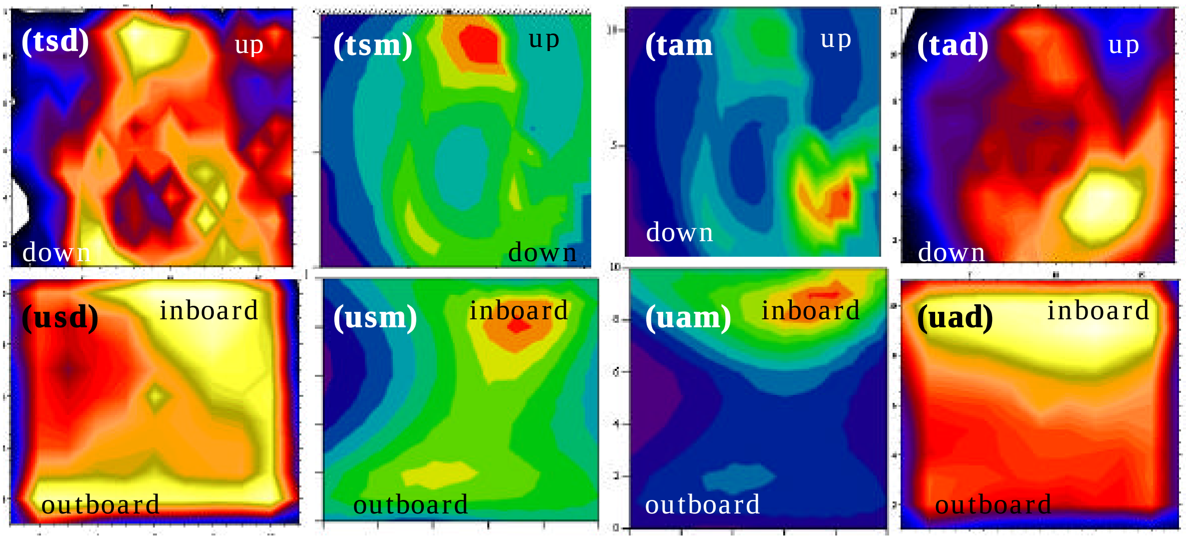

Fig. 9 IRVB radiation brightness image (d) data from (u) upper and (t) tangential ports during the (s) steady state and (a) asymmetric phases of the discharge compared with reconstructions from (m) model profiles.

4. Confinement in the high-density regime

Energy confinement time compared with ISS95 scaling declines in high-density and high-collisionality regime as shown in Fig. 10. This degradation mainly results from the loss of a strong, positive density dependence as in ISS95. Although the shallow penetration of the heating beams in the high-density regime is also a possible cause, it is not sufficient to explain the degradation from ISS95.

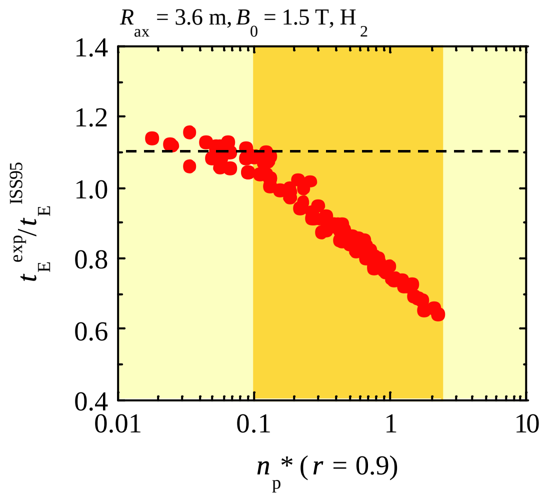

Fig. 10 Degradation from ISS95 in the high-collisionality regime.

In the gyro-Bohm model, the thermal diffusivity is predicted to increase with $T_e^{1.5}$. The dimensionless form of ISS95 has a gyro-Bohm like parameter dependence and this is reflected in the strong positive density dependence. The electron temperature dependence of the effective thermal diffusivity, c_e^{eff}, is shown in Fig. 11. In the high-collisionality (low-temperature) regime, a weak temperature dependence of $c_e^{eff} \propto T_e^{0.5}$ appears. As the temperature increases, a stronger temperature dependence as predicted by the gyro-Bohm model ($c_e^{eff} \propto T_e^{1.5}$) and/or neo-classical theory ($c_e^{eff} \propto T_e^{4.5}$) appears. These temperature dependences are observed independent of r. The weak temperature dependence of $c_e^{eff} \propto T_e^{0.5}$ leads to the weak density dependence of the energy confinement time of $t_E \propto \bar{n}_e^{1/3}$. Therefore, the degradation from ISS95 in the high-density regime can be attributed to the change in the temperature dependence of the thermal diffusivity.

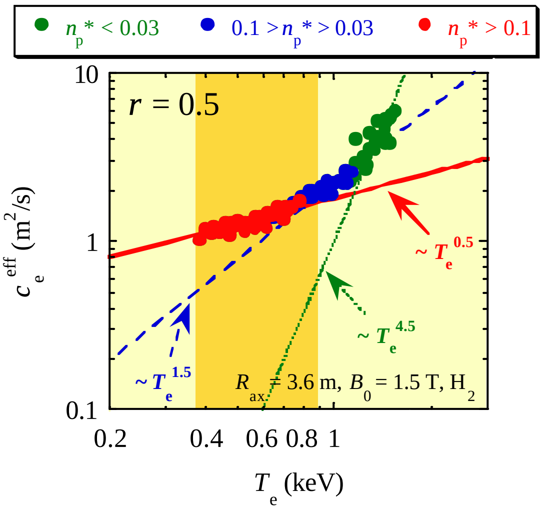

Fig. 11 Electron temperature dependence of the effective thermal diffusivity.

5. Discussion

That LHD plasmas can achieve high density steady state discharges at levels which are 1.4 times the Sudo limit has been confirmed with the most recent data taken at NBI powers of up to 11 MW. The assumption that the collapse of the plasma at the density limit is caused by a radiative thermal instability is supported by several observations. (1) There is a relationship between of the power dependence of the radiation on the density and the edge electron temperature. (2) As the plasma collapses, radiation from oxygen increases first (since it radiates at a higher temperature) followed by carbon (radiating at a lower temperature) which is the dominantly radiating intrinsic impurity. (3) Radiation profiles show that as the temperature drops and the plasma collapses, the radiating zone broadens and moves inward. Additional evidence that the poloidally asymmetric feature observed during the collapse is toroidally symmetric indicates that this phenomenon is a toroidal effect and not related to the geometry of the magnetic field nor of the vacuum vessel both of which are highly three-dimensional in LHD. Finally, studies show that confinement in the high density regime is degraded compared to ISS95 scaling. This degradation of confinement as density increases leads to an even more rapid drop in the temperature thereby more rapidly reaching the edge threshold temperature where the onset of the radiative thermal instability is triggered.

It is interesting that while LHD does not have any considerable plasma current which can disrupt and terminate the discharge at high density as in a tokamak, there are several common features of the density limiting phenomena in both types of devices. One is a role played by the edge plasma and the other is the MARFE-like asymmetries observed. Several questions remain unanswered regarding the collapse of the plasma in LHD. While we have evidence that the radiation from carbon is playing a key role in the radiative collapse, it is not clear if the rapid increase in radiation can be solely attributed to the dropping edge temperature leading to an increase in the cooling rate, or if the impurity density might be increasing due to some enhanced transport or recycling. Recent measurements of radial electric field during the collapse indicate that transition of the edge electric field from positive to negative due to increase of the density may be contributing to the inward flux of impurities [10]. Further clarification of these issues will require detailed transport modeling of spectroscopic data from during the plasma collapse.

[1] GREENWALD, M., Plasma Phys. Control. Fusion **44** (2002) R27.
[2] SUDO, S., et al., Nucl. Fusion **9** (1990) 11.
[3] GIANNONE, L., et al., Plasma Phys. Control. Fusion **42** (2000) 603.
[4] GIANNONE, L., et al., Plasma Phys. Control. Fusion **44** (2002) 2149.
[5] PETERSON, B.J., et al., Phys. Plasmas **8** (2001) 3861.
[6] XU, YUHONG, et al., Nucl. Fusion **42** (2002) 601.
[7] ASHIKAWA, N., et al., J. Nucl. Mater. **313-316** (2003) 1103.
[8] NISHIMURA, K., et al., J. Plasma Fusion Res. **79** (2003) 1216.
[9] PETERSON, B.J., et al., Plasma phys. Control. Fusion **45** (2003) 1167.
[10] IDA, K., et al., this conference.